Pergamon

Geochimica et Cosmochimica Acta, Vol. 67, No. 24, pp. 5071–5082, 2003

0016-7037/03 $30.00 + .00

doi:10.1016/S0016-7037(03)00205-9

Exsolution and coarsening in iron-free clinopyroxene during isothermal annealing

STEPHAN WEINBRUCH,* VOLKER STYRSA, and WOLFGANG FRIEDRICH MÜLLER

Institut für Angewandte Geowissenschaften, Technische Universität Darmstadt, Schnittspahnstr. 9, D-64287 Darmstadt, Germany

(*Received September* 30, 2002; *accepted in revised form January* 29, 2003)

Abstract—Exsolution and coarsening in Fe-free clinopyroxene of composition $En_{45.1}Di_{54.9}$ was studied at temperatures of 1300, 1200, and 1100°C, and annealing times between 10 min and 4320 h. Based on the wavelength of the exsolution lamellae, the exsolution process can be divided into exsolution sensu stricto and coarsening. During exsolution sensu stricto, the average wavelength of the "001" and "100" lamellae remains constant in contrast to the subsequent coarsening process. A progressive development of the microstructure is observed before coarsening which includes formation of island-like regions of dark contrast without phase separation, occurrence of pigeonite and diopside domains predominantly elongated along (100), formation of "100" exsolution lamellae, dissolution of the "100" lamellae, and predominant occurrence of "001" exsolution lamellae. All observations are in accordance with the exsolution mechanism of spinodal decomposition. After termination of the exsolution process, coarsening of the exsolution lamellae is observed. The "001" lamellae coarsen according to the rate law

$$\lambda_t^n - \lambda_0^n = n * k * exp(-\Delta H/RT) * (t - t_0),$$

with λ_t the average wavelength at time t, λ_0 the average wavelength at time t_0, ΔH an activation energy, R the gas constant, T the temperature [K], and n and k empirical constants.

From a multiple regression analysis the following values of the constants (± standard error) are obtained: $n = 2.86 \pm 0.15$, $k = 1.29*10^{14} \pm 3.41*10^8$ [$nm^{2.86}/h$], and $\Delta H = 80.34 \pm 1.76$ [kcal/mol]. The initial wavelength λ_0 was found to increase with increasing temperature (11.0 nm at 1100°C; 17.5 nm at 1200°C; 20.7 nm at 1300°C). The time t_0 to complete exsolution decreases with increasing temperature (60 h at 1100°C; 18 h at 1200°C; 8 h at 1300°C). The exponent n is within the error limits equal to 3, indicating volume diffusion as rate-controlling process. Coarsening of the exsolution lamellae was found to be substantially faster than reported in previous studies. *Copyright © 2003 Elsevier Ltd*

1. INTRODUCTION

Pyroxenes are a major constituent of many terrestrial and lunar rocks, as well as of most meteorites (Deer et al., 1978; Papike, 1998). Natural clinopyroxenes of intermediate composition within the pyroxene quadrilateral $CaMgSi_2O_6$ - $CaFeSi_2O_6$ - $Mg_2Si_2O_6$ - $Fe_2Si_2O_6$ are frequently exsolved into lamellae of Ca-rich and Ca-poor composition, i.e., augite or diopside with space group C2/c and pigeonite with space group $P2_1/c$ at room temperature (Buseck et al., 1980). Two main orientations of exsolution lamellae are observed: lamellae with composition planes close to (001) and close to (100). In previous literature, the lamellae are either termed "001" and "100" lamellae or lamellae on (001) and (100). In case of the "001" lamellae, the lattice relationships are $a_{augite} \parallel a_{pigeonite}$, $b_{augite} \parallel b_{pigeonite}$, $c^*_{augite} \parallel c^*_{pigeonite}$; for "100" lamellae the relationships are analogous (details are given by Skrotzki et al., 1991). It has been shown that the composition planes are not strictly parallel to (001) and (100), but commonly have irrational orientations, which is a consequence of minimizing the strain energy between host and lamellae (Robinson et al., 1977). The exact mechanism that operates during exsolution of clinopyroxene has not been constrained yet. It is generally believed that exsolution takes place either by spinodal decomposition or by nucleation and growth (Buseck et al., 1980; Putnis, 1992). However, the early stages of exsolution have not been studied systematically in silicate systems and, therefore, the two possible mechanisms cannot be distinguished easily, neither in experimental nor in natural samples.

The exsolution process is, in many cases, followed by coarsening of the exsolution lamellae. Because coarsening is diffusion-controlled and, thus time- and temperature-dependent, the periodicity (wavelength λ) of the exsolution lamellae can be used to infer cooling rates. Exsolution microstructures in clinopyroxene have been frequently used to constrain cooling rates of terrestrial and extraterrestrial rocks (Takeda et al., 1975; Grove, 1982; Watanabe et al., 1985; Brizi and Mellini, 1992; Weinbruch and Müller, 1995; McCallum and O'Brien, 1996; Weinbruch et al., 2001; Ferraris et al., 2002). Although the body of observations on exsolution phenomena in natural clinopyroxenes is continuously increasing, the experimental database for the cooling rate estimation is rather limited. The few studies which address the relation between the wavelength of the exsolution lamellae and the cooling rate (McCallister, 1978; Nord and McCallister, 1979; Grove, 1982; Fukuda et al., 1987; Weinbruch et al., 2001) were carried out on different pyroxene compositions and at different experimental conditions (e.g., isothermal annealing or continuous cooling).

Most estimates of cooling rates from clinopyroxene exsolution lamellae are based on the excellent and pioneering isothermal experiments of McCallister (1978). However, there are several reasons that justify (at least in our opinion) a reevaluation of his work. First, the early stages of the exsolution

* Author to whom correspondence should be addressed (dh6d@hrzpub.tu-darmstadt.de).

process were not studied in detail. Second, the two different processes of exsolution sensu stricto and coarsening of the exsolution lamellae were not distinguished. Thus, kinetics of these two processes was described with the same equation, which is certainly not appropriate. Third, it is desirable to have additional data on the coarsening kinetics to estimate cooling rates of natural samples more accurately.

The original motivation of our study was to obtain additional kinetic data on coarsening of clinopyroxene exsolution lamellae that can be applied to estimate cooling rates of chondrules more accurately (see discussion in Weinbruch and Müller, 1995). However, the system $Mg_2Si_2O_6$–$CaMgSi_2O_6$ is a well-characterized two-component system (Carlson, 1988, 1989) and a more detailed study of the development of exsolution is of general interest. The present study is, to the best of our knowledge, the most detailed experimental work on exsolution phenomena in pyroxenes and perhaps in silicates.

2. EXPERIMENTAL

All experiments were performed with synthetic iron-free clinopyroxene having a composition in the binary system $CaMgSi_2O_6$ - $Mg_2Si_2O_6$ (diopside–enstatite). For the high-pressure synthesis of the starting material (clinopyroxene solid solution with space group $P2_1/c$), a glass phase was synthesized from a mixture of SiO_2, CaO, and MgO. The oxides were mixed in a bowl mill for several hours. The material was melted in a furnace (Naber LHT 16/R) at 1550°C and subsequently quenched into water. To homogenize the starting material, the melting process was carried out nine times (the glass phase was crushed and mixed each time before melting). According to X-ray powder diffraction analysis and transmission electron microscopy (TEM), the obtained solid predominantly consisted of a glass phase with a minor amount (<5 vol.%) of crystalline material. The crystalline material is easily recognized by its white color and was removed. The composition and the homogeneity of the glass phase (after homogenizing and melting nine times) were determined by wavelength-dispersive X-ray microanalysis with a CAMECA CAMEBAX SX 50 electron microprobe. The composition of the glass phase was 54.9 ± 0.6 mol percent $CaMgSi_2O_6$ and 45.1 ± 0.8 mol percent $Mg_2Si_2O_6$ (mean value ± 1s standard deviation of 31 measurements).

The clinopyroxene solid solution was synthesized for 1.5 h at 30 kbar and 1550°C in a belt apparatus. For this purpose, the fine crushed glass was pressed into small Pt tubes with 3 mm diameter and 3 mm height. The Pt tubes were closed by welding. Details of the experimental setup are described elsewhere (Brey et al., 1990). Most isothermal annealing experiments were performed with material from synthesis run HPE7, three annealing experiments (72 h at 1200°C, 72 h and 120 h at 1300°C) with material from HPE9. An influence of the different starting materials on exsolution and coarsening phenomena was not observed. According to TEM, the clinopyroxene obtained in both synthesis runs consisted predominantly of a phase with space group $P2_1/c$; a minor amount (<5 vol.%) of a phase with space group C2/c was also observed.

To study exsolution and coarsening, the clinopyroxene samples were annealed in open Pt crucibles at atmospheric pressure between 10 min and 4320 h at a temperature of 1100°C, between 1 and 720 h at 1200°C, and between 1 and 360 h at 1300°C. The temperature was measured directly at the Pt crucibles using a Pt-PtRh10 thermocouple, which was repeatedly calibrated against the melting points of gold (1063°C) and silver (961°C), and against the orthorhombic/hexagonal phase transition in $BaCO_3$ (793°C; Weinbruch et al., 1992). From these experiments, accuracy of the annealing temperature is estimated to be ±2°C. The stability of temperature was ±2°C.

Small pieces of the annealed samples were crushed between glass slides and suspended with ethanol onto hole-containing carbon foils supported on TEM grids. TEM investigations were carried out with two different instruments: a Philips CM 12 operated at 120 kV, and for high-resolution imaging a Philips CM 20 operated at 200 kV. Both instruments are equipped with energy-dispersive X-ray detectors. The magnification of the CM 12 was calibrated using special TEM grids (lattice with 2160 lines per mm). Standard methods of TEM were employed: bright field imaging, dark field imaging, lattice imaging, selected area electron diffraction (SAED), and energy-dispersive X-ray microanalysis (EDX).

The wavelength (periodicity) of the lamellae was determined by measuring the widths of the pigeonite and diopside lamellae separately for "001" exsolution lamellae, and together for both phases for "100" lamellae. The width of each exsolution lamella ("001") or pair of lamellae ("100"), respectively, was measured repeatedly (up to 20 times) at different positions (at a distance of approximately 30 nm). For each sample, median and quartiles were calculated from the data of the individual pigeonite and diopside lamellae or pairs of lamellae, respectively.

Pigeonite ($P2_1/c$) and diopside (C2/c) areas in the annealed materials were distinguished by TEM methods due to their different Bravais lattices. Because the reflections h00 with h odd are allowed in P-lattices but forbidden in C-lattices, lattice imaging of h00 planes is a proper and comfortable method to discern between areas of P-lattice and C-lattice, even of unit cell widths, by the spacing of the h00 lattice planes. This spacing is ~9.2 Å (d_{100}) for pigeonite and 4.6 Å (d_{200}) for augite. Dark field images using h + k odd reflections can be used to distinguish the two different phases in lower resolution images. Distinction of Ca-rich (diopsidic) and Ca-poor (pigeonitic) areas by means of EDX was not possible because of the small size of the exsolution lamellae. Complementary studies with electron energy loss imaging filtering systems are in preparation.

3. RESULTS

The exsolution process can be divided into exsolution sensu stricto and coarsening of the exsolution lamellae. These two different processes are often not distinguished in the mineralogical literature (in contrast to material science), despite the fact that they can be easily recognized. During exsolution sensu stricto the average wavelength (periodicity of spacing) of the "001" and of the "100" exsolution lamellae remains constant in contrast to the coarsening process where the average wavelength of the exsolution lamellae increases during annealing (see below).

3.1. Exsolution Sensu Stricto

Exsolution in clinopyroxenes is more complex than expected and documented in previous literature. Before coarsening, a progressive development of characteristic microstructural features with annealing time is observed. Different stages of this continuous process are illustrated schematically in Figure 1. TEM images of the exsolution stages are given in Figures 2 and 3, electron diffraction patterns in Figure 4. Due to the slow kinetics, the different stages of the exsolution process can be best distinguished in samples annealed at 1100°C. However, even at this annealing temperature more than one stage may be observed in the same sample. At higher temperatures of 1200 and 1300°C, the progressive development of the microstructure cannot be recognized easily, as several stages of the exsolution process are generally observed at the same annealing time.

Incipient exsolution is characterized by island-like regions of dark contrast (Figs. 1a and 2a). According to (h00) lattice images (Fig. 3a) and SAED (Fig. 4a), phase separation did not yet occur at this stage of the exsolution process. The regions of dark contrast are mostly elongated approximately parallel to (100), a small number approximately parallel to (001). The deviation from the crystallographic planes is only a few degrees. The regions of dark contrast are distributed homoge-

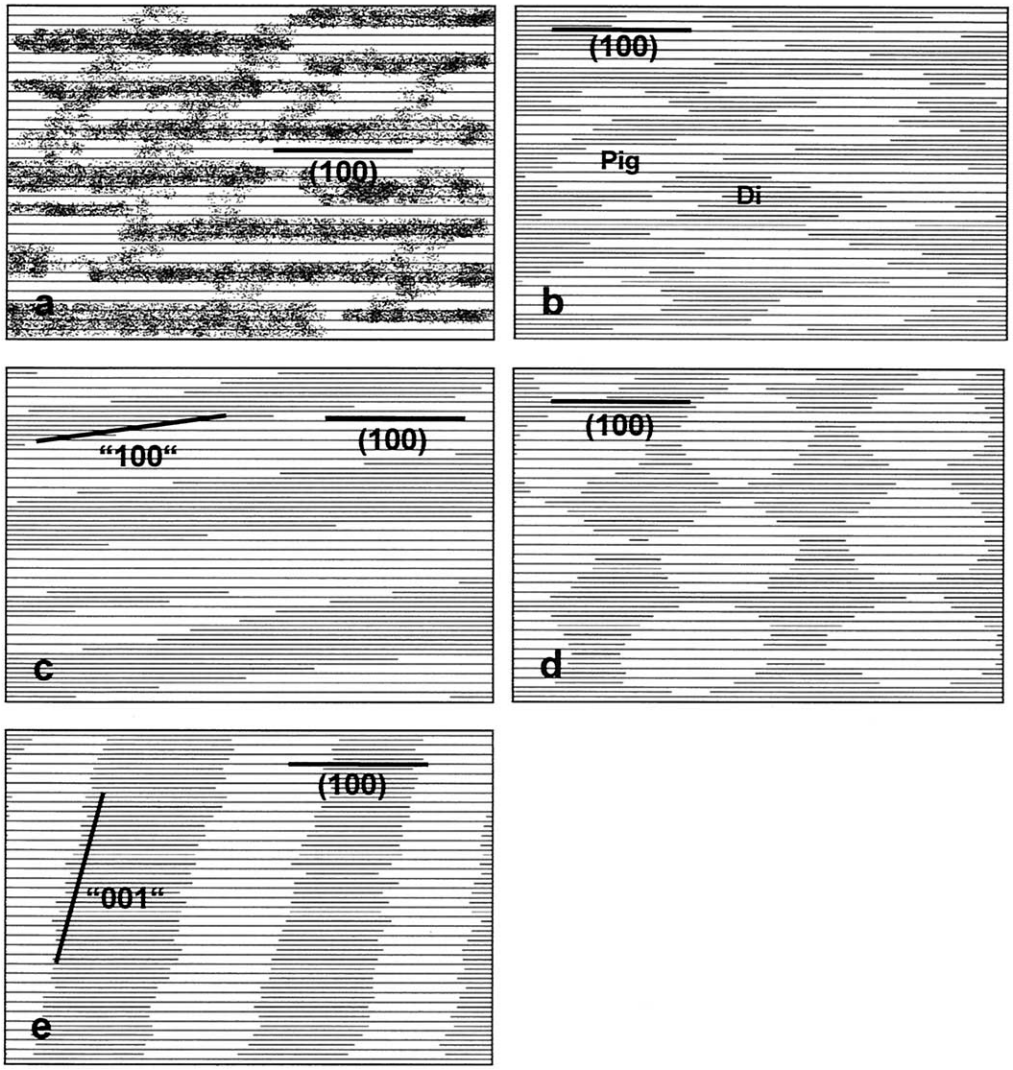

Fig. 1. Schematic illustration of the different exsolution stages: (a) formation of island-like regions of dark contrast without phase separation, (b) occurrence of pigeonite and diopside domains predominantly elongated along (100), (c) formation of "100" exsolution lamellae, (d) dissolution of the "100" lamellae, (e) predominant occurrence of "001" exsolution lamellae.

neously in the examined areas. Periodic structures are not observed. SAED reveals weak streaks of the reflections parallel **a*** (Fig. 4a). At 1100°C, the island-like regions of dark contrast are encountered at annealing times of 10, 20, and 40 min.

During further annealing, phase separation into diopside (space group C2/c) and pigeonite (space group $P2_1/c$) is observed (Figs. 1b and 3b). Both phases occur at equal abundance and form domains of approximately 6 * 60 nm size. The phase separation into diopside and pigeonite is first observed after 40 min annealing at 1100°C. The domains are predominantly elongated on (100); however, a significant fraction of the domains is oriented along (001) (Fig. 2b). Regions with exsolved features in two almost perpendicular directions look like the textile tweed (Fig. 2c) and are, thus, termed tweed textures. It should be emphasized here that the tweed textures already occur before the development of periodic exsolution lamellae. At 1100°C, tweed textures are most pronounced after 4 and 8 h annealing.

The island-like domains grow predominantly parallel to the (100) planes leading to "100" exsolution lamellae (Figs. 1c, 2d, and 3c). The first "100" lamellae are observed after 3 h annealing at 1100°C. The median of the wavelength of the "100" lamellae (≈4.5 nm at 1100°C) remains almost constant during the exsolution process. The observed development from island-like domains to exsolution lamellae (both predominantly oriented on (100)) leads to pronounced changes in the electron diffraction patterns. In areas with tweed texture, streaking of the reflections parallel **a*** and parallel **c*** is observed (Fig. 4b, c). During formation of the "100" exsolution lamellae, the intensity of streaks of a- and b-reflections parallel **a*** increases strongly and satellite reflections parallel **a*** arise.

In the further exsolution process (after 12 h annealing at

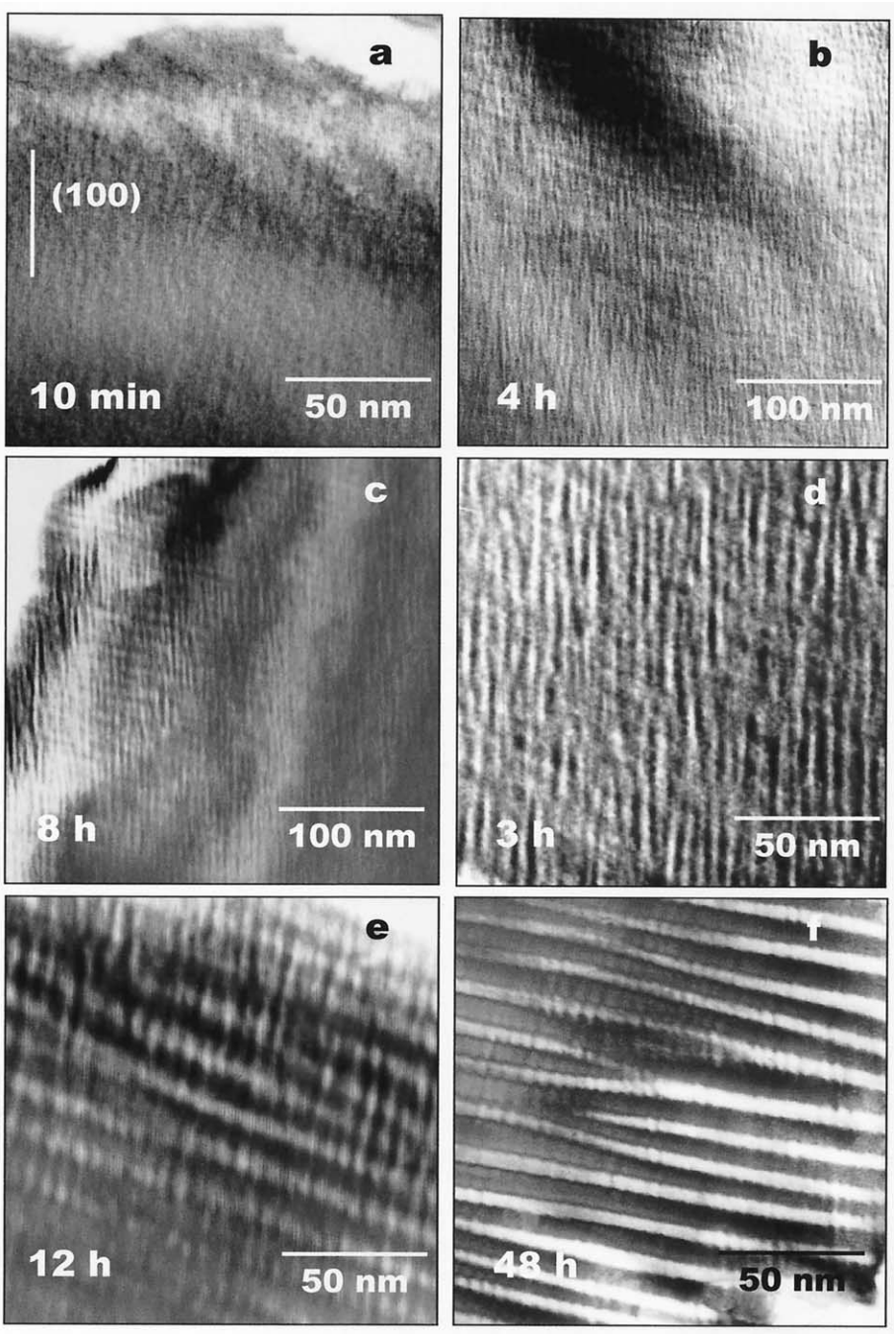

Fig. 2. TEM bright field images of exsolution features from samples annealed at 1100°C for different times. The orientation is identical in micrographs a–f.

1100°C), the "100" lamellae dissolve, and lamellae on "001" are forming (Figs. 1d, 2e). After completion of the exsolution process, only few "100" lamellae are encountered (Figs. 1e, 2f). Their abundance decreases with increasing temperature: $<5\%$ at 1100°C; $<2\%$ at 1200°C; $<1\%$ at 1300°C. The "001" lamellae formed during exsolution have diffuse phase boundaries between diopside and pigeonite (Figs. 2e, 2f, 3d) in contrast to lamellae that underwent subsequent coarsening (Fig. 5). The wavelength of the "001" lamellae remains constant during exsolution (Table 1). This almost constant wavelength and the diffuse phase boundaries are characteristic for the last stage of exsolution. Selected area electron diffraction in [001] orientation (Fig. 4d) revealed distinct streaking of all reflections parallel **c***. The intensity of the streaks parallel **a*** decreases substantially.

3.2. Coarsening

The boundary between exsolution sensu stricto and coarsening can be defined by analysis of the evolution of the lamellar

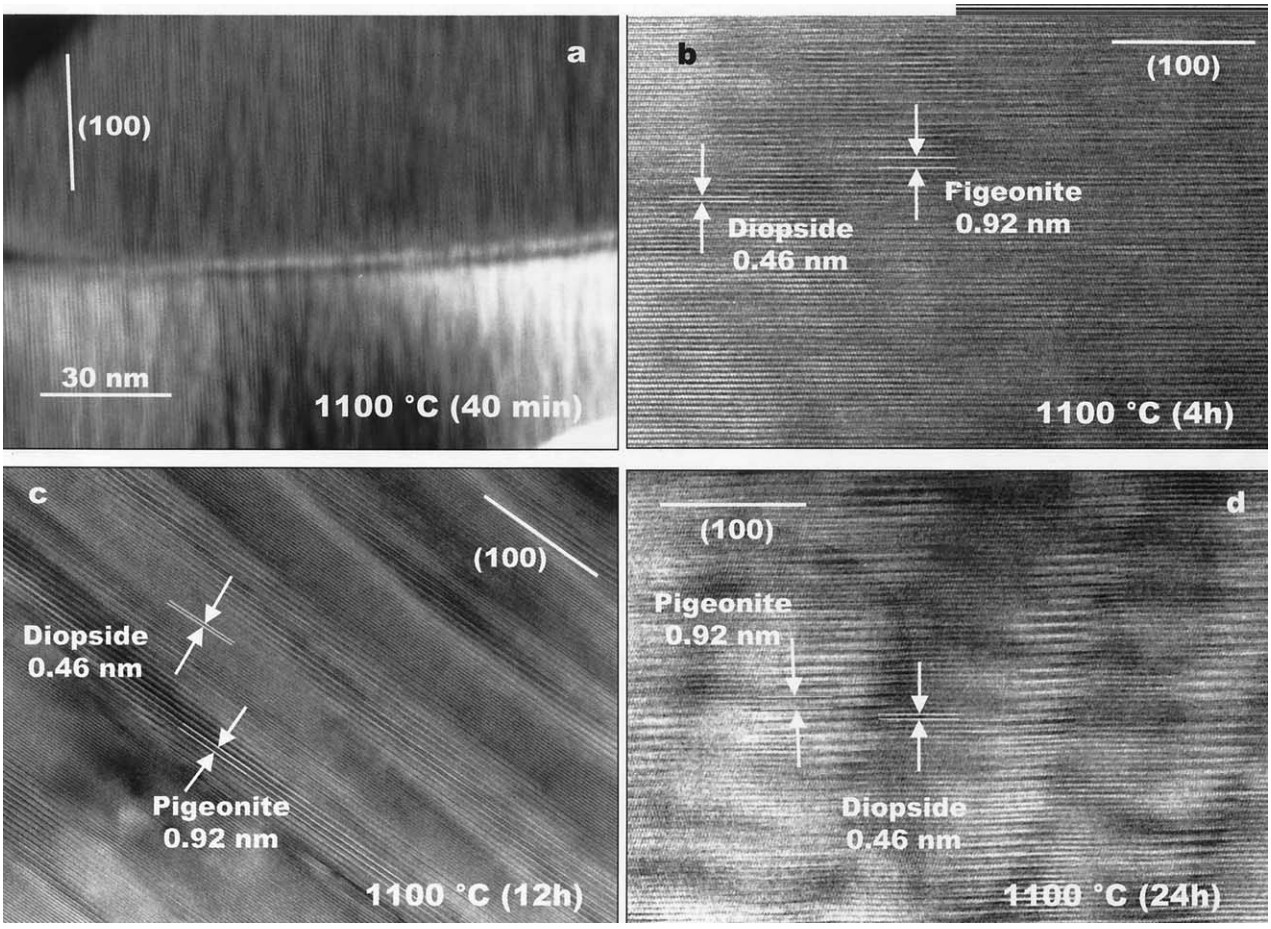

Fig. 3. TEM h00 lattice images of exsolution features from samples annealed at 1100°C.

spacings as a function of time (Table 1). At all three annealing temperatures, the wavelength λ of the "001" lamellae remains constant for a certain time period before it significantly increases. Therefore, it is reasonable to define the boundary between exsolution sensu stricto and coarsening as the time (t_0) where the constant wavelength (λ_0) starts to increase. The time t_0 (Table 1) was calculated as the mean value of the last annealing time with constant wavelength and the first annealing time where coarsened lamellae are observed. In accordance with theoretical predictions for spinodal decomposition (e.g., Cahn, 1968), the initial average wavelength λ_0 was found to increase with increasing temperature (Table 1).

There are two additional observations which support our definition of the boundary between exsolution and coarsening. First, at time t_0 almost all relicts of "100" exsolution lamellae are dissolved. Second, during the time period with constant wavelength, the phase boundary between pigeonite and diopside is rather diffuse (Figs. 2e, 2f, 3d), in contrast to the smooth appearance of coarsened lamellae (Fig. 5).

The development of the microstructure during coarsening is illustrated in Figure 5 for an annealing temperature of 1100°C. The wavelengths of the "001" lamellae as a function of temperature and annealing time are given in Table 1. The empirical size distributions of the pigeonite and the diopside lamellae and their implications for the derivation of the coarsening process will be published elsewhere.

Splitting of the reflections $h + k$ even parallel **c*** (in [001] orientation) into separate reflections for the diopside and pigeonite structure is only observed in the coarsened "001" lamellae (Fig. 4e, f). This splitting is due to the different monoclinic angles β of the diopside and the pigeonite lattice.

Coarsening of the "001" exsolution lamellae can be described by the following empirical equation (Carpenter, 1991):

$$\lambda_t^n - \lambda_0^n = n * k * exp(-\Delta H/RT) * (t - t_0), \qquad (1)$$

with λ_t the average wavelength at time t, λ_0 the average wavelength at time t_0, ΔH an activation energy, R the gas constant, T the temperature [K], and n and k empirical constants. The experimental data (Table 1) were fitted directly to Eqn. 1, and the following values for the constants (± standard error) were obtained from a multiple regression analysis: n = 2.86 ± 0.15; $k = 1.29 * 10^{14} \pm 3.41 * 10^8$ [$nm^{2.86}$/h]; ΔH = 80.34 ± 1.76 [kcal/mol].

As for the "001" lamellae, the wavelength of the "100" lamellae remains constant during exsolution sensu stricto and then increases during further annealing (Table 2). Due to the limited number of "100" lamellae observed at 1200 and 1300°C, this behavior could only be documented at a temper-

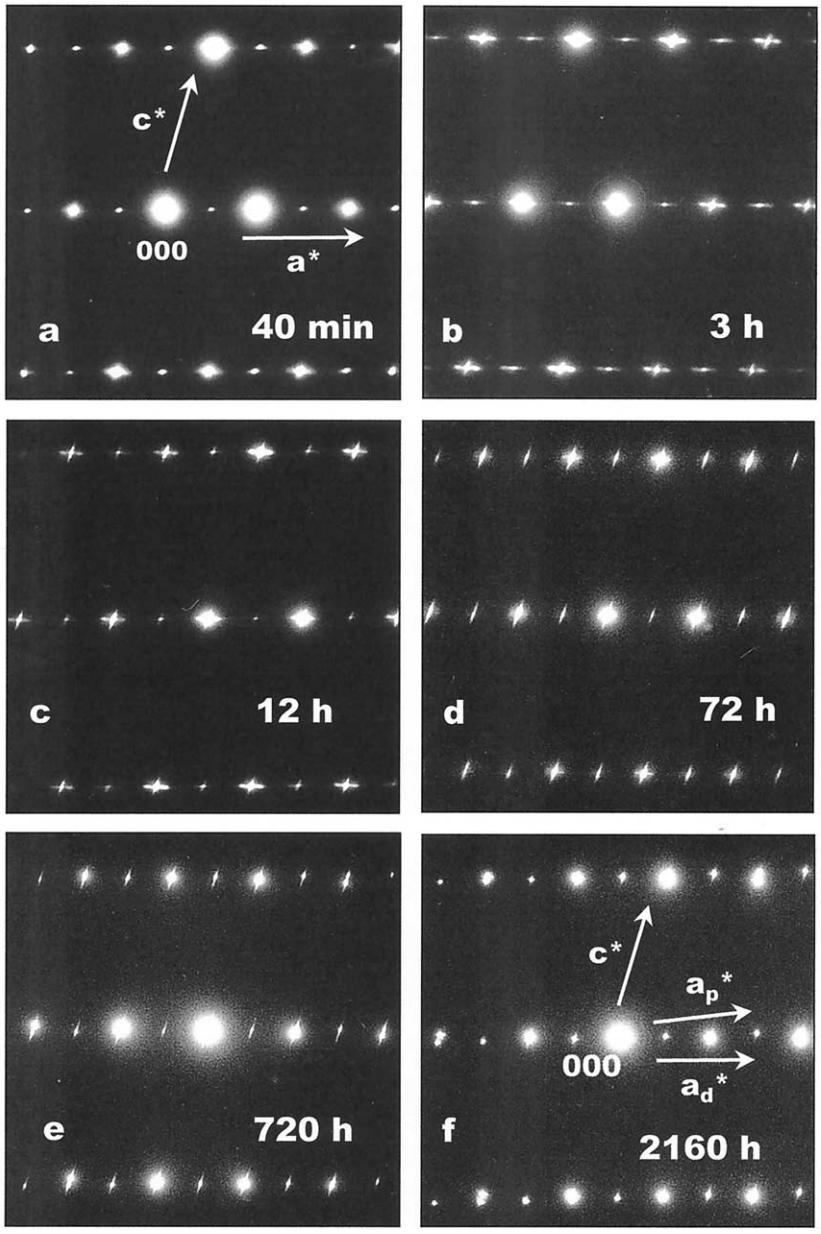

Fig. 4. Electron diffraction patterns (orientation [001]) from samples annealed at 1100°C.

ature of 1100°C. The small number of observations prevented a quantitative treatment of the coarsening kinetics of the "100" exsolution lamellae.

3.3. Twinning and Antiphase Domains

In the annealed samples, occasionally twins on (100) were encountered (Fig. 5a). Antiphase domains (APDs) with the displacement vector 1/2(**a** + **b**) were found in the pigeonite lamellae. Their formation is due to the transformation of high ($C2/c$) to low ($P2_1/c$) pigeonite by which the translational symmetry 1/2(**a** + **b**) is lost. The APDs are elongated parallel to the crystallographic (100) planes.

4. DISCUSSION

4.1. Exsolution Sensu Stricto

Exsolution may take place by the three different processes of heterogeneous nucleation, homogeneous nucleation, or spinodal decomposition (Buseck et al., 1980; Putnis, 1992). Heterogeneous nucleation can be excluded for our experiments, as enrichment of exsolution lamellae along defects (including grain boundaries and the sample surface) is not observed.

Exsolution of clinopyroxene by the mechanism of spinodal decomposition has been reported in many papers (e.g., Champness and Lorimer, 1971, 1976; McCallister and Yund, 1975, 1977; Buseck et al., 1980; Jantzen, 1984). Spinodal decompo-

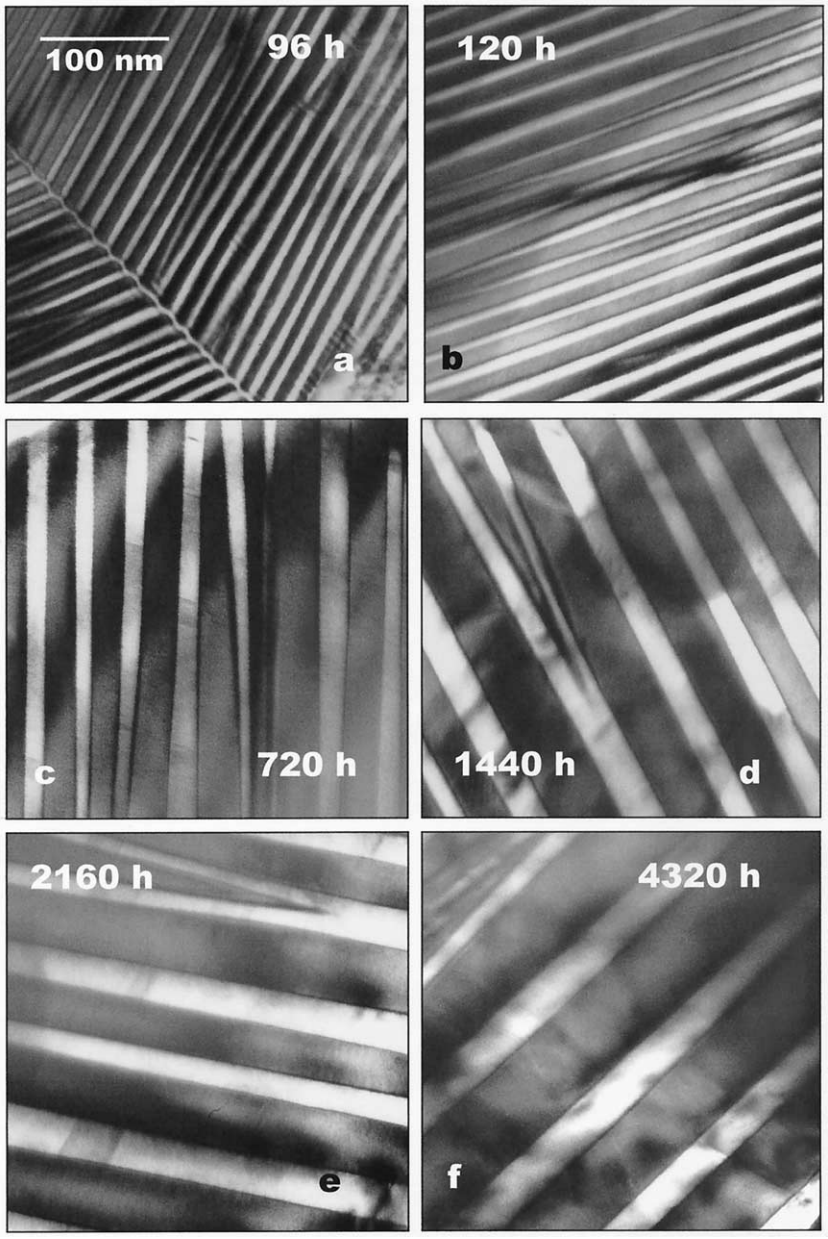

Fig. 5. TEM bright field images of coarsened "001" lamellae (1100°C). Bright lamellae are pigeonite, dark lamellae diopside.

sition as exsolution mechanism is generally deduced from textural features such as the presence of modulated textures or tweed textures (Champness and Lorimer, 1971, 1976; Lally et al., 1975; Nord et al., 1976; Buseck et al., 1980) or the occurrence of diffuse interfaces between the solute-rich and solute-poor component in the initial stage of exsolution (Champness and Lorimer, 1976; Buseck et al., 1980). However, it should be kept in mind that to unequivocally prove the mechanism of spinodal decomposition, one must verify that the amplitude of the composition waves increases with time (uphill diffusion). Such a proof by microanalytical techniques has not yet been presented for silicates.

All observations of the present study are in accordance with the model of spinodal decomposition. A strong hint for this process is the fact that phase separation did not occur in the early stage of exsolution (Cahn, 1968). The islands of dark contrast (Figs. 2a, 3a) are most likely caused by chemical fluctuations which lead to small changes in the lattice constants. According to lattice imaging (Fig. 3a), the samples are not exsolved into pigeonite and diopside at this early stage.

The diffuse interfaces between the exsolved phases also indicate that exsolution took place by spinodal decomposition. According to Buseck et al. (1980), nucleation leads to a distinct interface at the onset of exsolution. In contrast, the compositional modulations during spinodal decomposition lead to a diffuse interface during the early stages of exsolution, which

Table 1. Wavelength of "001" exsolution lamellae.

	Wavelength (nm)				
Time (h)	Median	Lower and upper quartile	n (Di)[a]	n (Pig)[b]	Process
1100°C: λ_0 = 11.0 nm; t_0 = 60 h					
12	10.59	(10.59–12.18)	151	131	exs.
18.5	11.65	(10.59–13.06)	107	107	exs.
24	10.87	(9.75–14.32)	347	326	exs.
48	11.06	(10.80–14.38)	217	209	exs.
72	13.36	(11.47–14.97)	480	469	coars.
96	20.13	(15.78–25.44)	222	217	coars.
120	21.69	(18.21–25.13)	102	101	coars.
360	34.83	(28.54–47.18)	140	142	coars.
720	40.68	(34.78–49.96)	143	145	coars.
1440	50.56	(39.48–60.34)	188	194	coars.
2160	56.51	(43.88–71.42)	146	157	coars.
4320	74.71	(59.27–94.78)	171	178	coars.
1200 °C: λ_0 = 17.5 nm; t_0 = 18 h					
8	16.88	(13.19–19.04)	164	157	exs.
12	18.18	(14.73–21.36)	197	178	exs.
24	22.39	(19.73–25.92)	170	166	coars.
48	26.95	(21.64–30.30)	93	92	coars.
72	37.21	(31.57–45.38)	152	155	coars.
96	40.54	(31.89–51.24)	168	166	coars.
120	37.96	(30.27–46.10)	246	241	coars.
120	28.02	(23.76–38.79)	188	189	coars.
240	51.46	(40.33–65.30)	134	137	coars.
360	81.67	(64.91–102.39)	103	106	coars.
360	70.79	(57.18–92.40)	30	31	coars.
720	95.99	(75.83–115.68)	104	102	coars.
1300 °C: λ_0 = 20.7 nm; t_0 = 8 h					
2	19.40	(16.88–21.01)	85	87	exs.
3	22.00	(19.16–25.10)	227	218	exs.
4	20.59	(17.36–24.96)	138	130	exs.
12	31.32	(27.18–38.09)	144	135	coars.
24	51.47	(44.62–60.88)	101	101	coars.
72	65.77	(48.42–86.30)	176	174	coars.
120	75.79	(64.67–94.70)	138	130	coars.
360	118.54	(94.99–142.31)	114	121	coars.

exs. = exsolution; coars. = coarsening.
[a] n(Di) = number of diopside lamellae measured.
[b] n(Pig) = number of pigeonite lamellae measured.

becomes distinct and sharp at the end of the exsolution process (before coarsening).

The occurrence of modulated structures and tweed structures is—if derived from a later stage of the exsolution process—not a strong constraint for spinodal decomposition. According to Wagner and Kampmann (1991), such textures may also form by totally different mechanisms (e.g., strong elastic interaction of a high number density of nuclei). However, together with the other observations mentioned above, the tweed textures encountered in the present study (Fig. 2c) nicely fit into the overall picture of spinodal decomposition.

The observed dependence of the initial wavelength λ_0 on temperature (Table 1) also supports the mechanism of spinodal decomposition. A theoretical treatment of spinodal decomposition (Cahn, 1968) leads to the prediction that λ_0 decreases with decreasing temperature, which is in accordance with our experimental data.

The different exsolution stages that are observed with increasing annealing time (Fig. 1) clearly demonstrate that the "001" lamellae have the energetically favored orientation at the temperatures investigated. This conclusion is in agreement with

Table 2. Wavelength of "100" exsolution lamellae.

	Wavelength (nm)			
Time (h)	Median	Lower and upper quartile	n[a]	Process
1100°C				
3	4.24	(4.24–4.24)	59	exs.
8	4.13	(4.13–5.17)	57	exs.
12	4.26	(4.24–4.39)	120	exs.
24	4.37	(4.37–4.37)	27	exs.
72	5.48	(4.39–6.58)	27	exs.
360	23.50	(19.34–31.48)	15	coars.
720	16.18	—	7	coars.
2160	26.62	(24.69–36.06)	17	coars.
4320	27.32	(20.04–36.61)	16	coars.
1200°C				
4	4.35	(4.35–6.52)	84	exs.
12	28.10	(23.76–31.52)	12	coars.
72	21.11	(14.20–25.11)	20	coars.
1300°C				
3	8.33	(8.33–8.33)	18	exs.
24	17.10	(13.77–18.05)	4	coars.
360	49.38	(27.43–84.12)	4	coars.

exs. = exsolution, coars. = coarsening.
[a] n = number of pairs of lamellae measured.

the dominance of the "001" lamellae in natural clinopyroxenes frequently reported in the literature (e.g., Buseck et al., 1980). Our TEM investigations show that all the lamellae observed during exsolution sensu stricto are fully coherent, dislocations were never encountered. An important consequence of coherency is that both phases are elastically strained and that the orientation of the lamellae will be such as to minimize the elastic strain energy (Morimoto and Tokonami, 1969; Tullis and Yund, 1979). Both, lattice misfit and elastic anisotropy for both phases must be minimized to minimize the elastic strain energy (Willaime and Brown, 1974). However, the contribution of the elastic anisotropy to the orientation of lamellae in clinopyroxene is small in comparison to the effect of lattice misfit (Tullis and Yund, 1979). To calculate the solvus of Fe-free clinopyroxenes, Tullis and Yund (1979) introduced a molar strain energy coefficient, which turned out to be 0.650 kcal/mol for the "001" orientation and 1.060 kcal/mol for the "100" orientation. According to Buseck et al. (1980), the lower elastic strain energy for the "001" lamellae is consistent with the observation that this orientation is dominating in natural samples. Thus, we conclude that the lower elastic strain energy is also responsible for the observed dominance of the "001" orientation at longer annealing times.

The observed change of the orientation of the exsolution lamellae with annealing time is not yet understood. It may be speculated that the "100" lamellae are kinetically favored at the initial stages of exsolution due to the smaller wavelength which leads to shorter diffusion distances and to higher gradients of the chemical potential. In addition, anisotropy of diffusion in clinopyroxene may also play a role. However, it should be emphasized here that a rigorous theoretical treatment is beyond the scope of this paper and is left for further studies.

4.2. Coarsening

After termination of the exsolution process, coarsening of the exsolution lamellae is observed. At all three annealing temperatures, coarsening was found to be much faster in our experiments compared with the results of McCallister (1978). At longer annealing times, the difference in the observed wavelength may be more than a factor of 2 (the example of 1100°C is given in Fig. 6). The reasons for this discrepancy are not known.

The initial wavelength λ_0 (i.e., the wavelength before coarsening) as well as the time t_0 (i.e., the time to terminate exsolution) obtained in the present study are almost identical to the findings of McCallister (1978), at least if the original data points are compared (Fig. 6b). The pioneering experimental work of McCallister (1978) was focused on the coarsening process. Therefore, only a small number of short-time experiments were performed and the period of constant wavelength before coarsening was not detected. Together with our data, however, the constant wavelength during exsolution sensu stricto is quite obvious (Fig. 6b).

Exsolution and coarsening were not distinguished by McCallister (1978), and kinetics of both processes was described with the same equation:

$$\lambda_t - \lambda_0 = k * t^{1/3}, \qquad (2)$$

with λ_t the average wavelength at time t, λ_0 the initial wavelength, and k a constant. The values for the initial wavelength given in his paper (1100°C: λ_0 = 5.3 nm; 1200°C: λ_0 = 8.9 nm; 1300°C: λ_0 = 10.9 nm) are not compatible with the present study (Table 1). Unfortunately, it is not clear how λ_0 was derived by McCallister (1978). If the experimental data of McCallister (1978) are fitted to the equation used by him to describe the coarsening kinetics (Eqn. 2), it appears that λ_0 is almost independent of temperature: 9.0 nm at 1100°C, 8.8 nm at 1200°C, and 11.5 nm at 1300°C (Fig. 2 of his paper was scanned to obtain the individual data points) in contrast to the theoretical predictions for spinodal decomposition (Cahn, 1968). It should be mentioned in this context that accurate data for λ_0 and t_0 are required to constrain high cooling rates where coarsening is not pronounced (see the discussion of cooling rates of chondrules by Weinbruch and Müller, 1995).

The rate law (Eqn. 2) used by McCallister (1978) is often confused with the rate law resulting from the Lifshitz and Slyozov (1961) and Wagner (1961) theory. In this approach (generally referred to as LSW theory), it is assumed that the

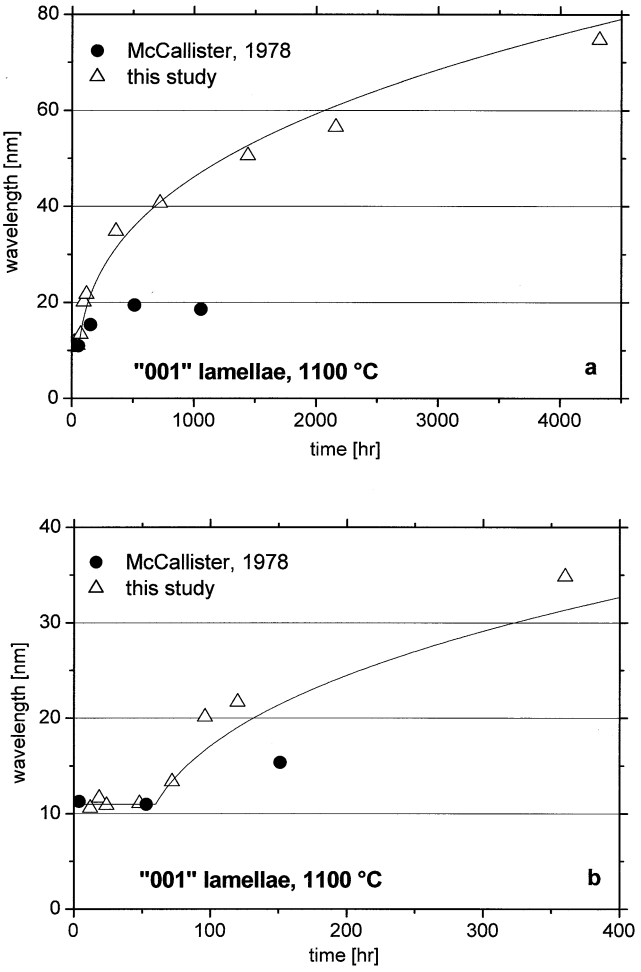

Fig. 6. Wavelength of "001" exsolution lamellae as function of annealing time at a temperature of 1100°C (experimental results of McCallister, 1978 and the present study). (a) All annealing times. (b) Enlargement of short time experiments (up to 400 h). The results of fitting the wavelength data of this study to Eqn. 1 are shown as solid line.

precipitates are spherical and that the mean particle distance is far exceeding their size. It is further supposed that the system is highly diluted (i.e., the volume fraction of the precipitates is close to zero) and that the decomposition is close to completion (i.e., the supersaturation is approximately zero). Under these conditions, the coarsening rate of the average particle size *dr/dt* is proportional to $1/r^2$ which yields a rate law of the form:

$$r_t^3 - r_0^3 = k * t, \tag{3}$$

with r_t the average particle radius at time t, r_0 the average radius at $t = 0$, and k a constant. According to Doherty (1982), the same type of equation can be used to describe coarsening of plates. It should be emphasized here that Eqns. 2 and 3 are only the same for the boundary conditions $r >> r_0$ and $t >> t_0$, respectively (Murty, 1969). Despite the fact that these boundary conditions are often not fulfilled in natural samples, Eqn. 2 is frequently used in mineralogy to describe coarsening kinetics of exsolution lamellae (e.g., McCallister, 1978; Yund and Davidson, 1978; Grove, 1982; Yund, 1983; Putnis, 1992).

An alternative approach to describe the coarsening kinetics of exsolution lamellae was published by Brady (1987). In this approach it is assumed that diffusional exchange between the wedge-shaped terminations of the exsolution lamellae and the large flat sides of adjacent lamellae is the principal coarsening mechanism. The driving force is then inversely proportional to the lamellar wavelength (see also Cline, 1971) and a parabolic rate law for coarsening is obtained:

$$\lambda_t^2 - \lambda_0^2 = k * t. \tag{4}$$

In most previous papers on coarsening of exsolution lamellae the exponent in the rate law was imposed by the use of a certain equation. In contrast, we decided to use Eqn. 1 to determine the exponent directly from the experimental data (this equation was used by Carpenter (1991) to describe the coarsening kinetics of type b antiphase domains in anorthite). A multiple regression analysis yielded an exponent of 2.86 $\pm$ 0.15 (standard error), which is within the error limits equal to 3. An exponent of 3 is generally thought to indicate volume diffusion as the rate-controlling process (Martin and Doherty, 1976; Doherty, 1983; Gleiter, 1983; Joesten, 1991; Wagner and Kampmann, 1991).

4.3. Implications for Chondrule Cooling Rates

Lamellar exsolution microstructures in clinopyroxene have been used by several authors to constrain cooling rates of chondrules (Kitamura et al., 1983, 1986; Watanabe et al., 1985; Müller, 1991; Müller et al., 1995; Weinbruch and Müller, 1995; Weinbruch et al., 2001). The predominant development of coherent "001" lamellae in clinopyroxene requires cooling rates below approximately 50 to 60°C/h; modulated structures are formed at higher cooling rates between 50 and 450°C/h (Weinbruch et al., 2001).

In chondrules, exsolution lamellae are mostly observed in Fe-bearing clinopyroxene (Weinbruch et al., 2001). One exception are granular olivine pyroxene (GOP) chondrules from the Allende CV3 chondrite, in which exsolution of almost Fe-free clinopyroxene (Fs $\leq$ 3 mol %) was observed (Müller, 1976; Müller, 1991, Müller et al., 1995; Weinbruch and Müller, 1995). For these grains, coarsening of the "001" exsolution lamellae during cooling was modeled by Weinbruch and Müller (1995) using the isothermal growth rates determined by McCallister (1978), and cooling rates between 2 and 25°C/h were obtained for the temperature interval of 1350–1200°C. In the present study, coarsening of the "001" exsolution lamellae was found to be much faster than reported by McCallister (1978). Therefore, higher cooling rates should result if our new experimental data are applied. However, this is only true if the lamellar wavelength observed in a sample is significantly larger than the initial wavelength λ_0. This is illustrated in Figure 7, where the time dependence of the "001" lamellae wavelength, calculated with different equations, is shown for a temperature of 1300°C. Plotted are the wavelengths obtained from Eqn. 2 using the experimental data of McCallister (1978) and those received from Eqn. 1 using the kinetic data of the present study.

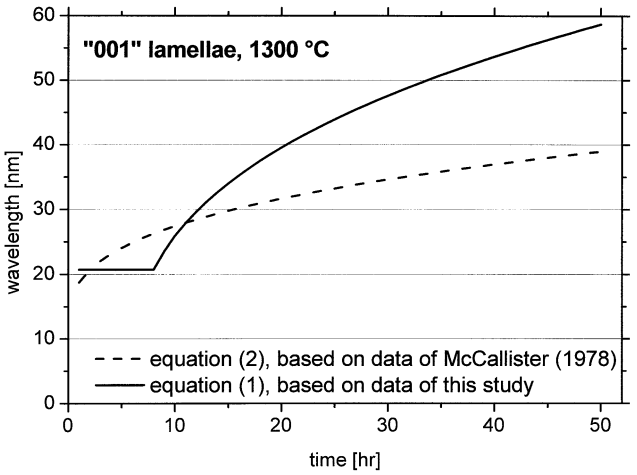

Fig. 7. Development of "001" lamellae with annealing time at 1300°C, calculated with different equations and using different experimental data.

As expected, for longer annealing times (e.g., exceeding approximately 11 h at 1300°C) Eqn. 1 yields higher wavelengths than Eqn. 2. However, at shorter annealing times, the opposite is true, as we have observed a period of constant wavelength before coarsening. Therefore, our new kinetic data will only result in higher cooling rates (compared with the use of the McCallister (1978) data) if the observed final wavelength, from which the cooling rate is inferred, exceeds the initial wavelength λ_0 substantially. In Allende GOP chondrules, the wavelength of "001" lamellae in clinopyroxene varied between 25 and 33 nm (Müller et al., 1995; Weinbruch and Müller, 1995). This value is close to the wavelength of the intersection of the two curves in Figure 7, which implies that the cooling rates of Allende GOP chondrules will not change substantially (compared with the estimate of Weinbruch and Müller, 1995), if the kinetic data of the present study are applied. Indeed, cooling rates between 1 and 10°C/h are obtained from time-temperature-transformation (TTT) diagrams for Allende GOP chondrules. This range is practically (i.e., within the error limits) identical with the estimate of 2–25°C/h determined by Weinbruch and Müller (1995) using the experimental data of

McCallister (1978). However, it should be emphasized here that for larger exsolution lamellae (e.g., from lunar and terrestrial rocks) the cooling rates will be substantially higher if the estimates are based on the results of the present study rather than on McCallister (1978).

Acknowledgments—This paper is dedicated to Robert Walker. S.W. and V.S. experienced and highly enjoyed the unique and stimulating spirit on the "fourth floor" at the McDonnell Center of the Space Sciences, which developed under the auspices of Robert Walker.

We would like to thank G. Brey for access to and help with the belt apparatus, and H. Fuess and G. Miehe for the use of the Philips CM20 transmission electron microscope. We also wish to thank S. Chakraborty and W. Schmahl for helpful discussions, and R. Harrison and an anonymous reviewer for thoughtful reviews of the manuscript. Financial support by the Deutsche Forschungsgemeinschaft is gratefully acknowledged.

Associate editor: S. Russell

REFERENCES

Brady J. B. (1987) Coarsening of fine-scale exsolution lamellae. *Am. Mineral.* **72**, 697–706.

Brey G. P., Weber R., and Nickel K. G. (1990) Calibration of a belt apparatus to 1800°C and 6 GPa. *J. Geophys. Res.* **95**, 15603–15615.

Brizi E. and Mellini M. (1992) Kinetical modelling of exsolution textures in igneous pyroxenes. *Acta Vulcan.* **2**, 87–93.

Buseck P. R., Nord G. L., and Veblen D. R. (1980) Subsolidus phenomena in pyroxenes. In *Pyroxenes* (ed. C. T. Prewitt), *Reviews in Mineralogy* **7,** 117–211. Mineralogical Society of America.

Cahn J. W. (1968) Spinodal decomposition. *Trans. AIME* **242**, 166–180.

Carlson W. D. (1988) Subsolidus phase equilibria on the forsterite-saturated join $Mg_2Si_2O_6$ –$CaMgSi_2O_6$ at atmospheric pressure. *Am. Mineral.* **73**, 232–241.

Carlson W. D. (1989) Subsolidus phase equilibria near the enstatite-diopside join in CaO-MgO-Al_2O_3-SiO_2 at atmospheric pressure. *Am. Mineral.* **74**, 325–332.

Carpenter M. A. (1991) Mechanisms and kinetics of Al-Si ordering in anorthite: I. Incommensurate structure and domain coarsening. *Am. Mineral.* **76**, 1110–1119.

Champness P. E. and Lorimer G. W. (1971) An electron microscopic study of a lunar pyroxene. *Contr. Mineral. Petrol.* **33**, 171–183.

Champness P. E. and Lorimer G. W. (1976) Exsolutions in silicates. In *Electron Microscopy in Mineralogy* (ed. H. R. Wenk), pp. 174–204. Springer Verlag.

Cline H. E. (1971) Shape instabilities of eutectic composites at elevated temperatures. *Acta Metall.* **19**, 481–490.

Deer W. A., Howie R. A., and Zussman J. (1978) *Rock-Forming Minerals Vol. 2a, Single-Chain Silicates*, 2nd ed. Longman.

Doherty R. D. (1982) Role of interfaces in kinetics of internal shape changes. *Met. Sci.* **16**, 1–13.

Doherty R. D. (1983) Diffusive phase transformations in the solid state. In *Physical Metallurgy*, 3rd ed. (eds. R. W. Cahn and P. Haasen), pp. 933–1030. Mineralogical Society of America.

Ferraris C., Folco L., and Mellini M. (2002) Chondrule thermal history from unequilibrated H chondrites: A transmission and analytical electron microscopy study. *Meteoritics Planet. Sci.* **37**, 1299–1321.

Fukuda K., Yamanaka T., and Tokonami M. (1987) Dependence of exsolution textures in synthetic augite on its composition and cooling rate. *Mineralog. J.* **13**, 376–389.

Gleiter H. (1983) Microstructure. In *Physical Metallurgy*, 3rd ed. (eds. R. W. Cahn and P. Haasen), pp. 649–712. Elsevier.

Grove T. L. (1982) Use of exsolution lamellae in lunar clinopyroxenes as cooling rate speedometers: An experimental calibration. *Am. Mineral.* **67**, 251–268.

Jantzen C. M. (1984) On spinodal decomposition in Fe-free pyroxenes. *Am. Mineral.* **69**, 277–282.

Joesten R. L. (1991) Kinetics of coarsening and diffusion-controlled mineral growth. In *Contact Metamorphism* (ed. C. D. M. Kerrick), *Reviews in Mineralogy* **26,** 507–582. Mineralogical Society of America.

Kitamura M., Yasuda M., Watanabe S., and Morimoto N. (1983) Cooling history of pyroxene chondrules in the Yamamoto-74191 chondrite (L3)—An electron microscopic study. *Earth Planet. Sci. Lett.* **63**, 189–201.

Kitamura M., Isobe H., Watanabe S., and Morimoto N. (1986) Analytical transmission electron microscopy of the Allende meteorite. *J. Electron Microsc.* **35**, 384–394.

Lally J. S., Heuer A. H., Nord G. L. Jr., and Christie J. M. (1975) Subsolidus reactions in lunar pyroxenes: An electron petrographic study. *Contrib. Mineral. Petrol.* **51**, 263–281.

Lifshitz I. M. and Slyozov V. V. (1961) The kinetics of precipitation from supersaturated solid solutions. *J. Phys. Chem. Solids* **19**, 35–50.

Martin J. W. and Doherty R. D. (1976) *Stability of Microstructure in Metallic Systems.* Cambridge University Press.

McCallister R. H. (1978) The coarsening kinetics associated with exsolution in an iron-free clinopyroxene. *Contr. Mineral. Petrol.* **65**, 327–331.

McCallister R. H. and Yund R. A. (1975) Kinetics and microstructure of pyroxene exsolution. *Carnegie Inst. Washington Year Book* **74**, 433–436.

McCallister R. H. and Yund R. A. (1977) Coherent exsolution in Fe-free pyroxenes. *Am. Mineral.* **62**, 721–726.

McCallum I. S. and O'Brien H. E. (1996) Stratigraphy of the lunar highland crust: Depths of burial of lunar samples from cooling-rate studies. *Am. Mineral.* **81**, 1166–1175.

Morimoto N. and Tokonami M. (1969) Oriented exsolution of augite in pigeonite. *Am. Mineral.* **54**, 1101–1117.

Müller W. F. (1976) Low-Fe clinopyroxenes along the join $MgSiO_3$-$CaMgSi_2O_6$ in the Allende meteorite. *Naturwissenschaften* **63**, 432.

Müller W. F. (1991) Microstructure of minerals in a chondrule from the Allende meteorite. II. Thermal history deduced from clinopyroxenes and other minerals. *Neues Jahrbuch Min. Abh.* **162**, 237–259.

Müller W. F., Weinbruch S., Walter R., and Müller-Beneke G. (1995) Transmission electron microscopy of chondrule minerals in the Allende meteorite: Constraints on the thermal and deformational history of granular olivine-pyroxene chondrules. *Planet. Space Sci.* **43**, 469–483.

Murty H. N. (1969) Kinetics of grain growth. *Phil. Mag.* **20**, 855–858.

Nord G. L., Heuer A. H., and Lally J. S. (1976) Pigeonite exsolutions from augite. In *Electron Microscopy in Mineralogy* (ed. H. R. Wenk), pp. 220–227. Springer Verlag.

Nord G. L. and McCallister R. H. (1979) Kinetics and mechanisms of decomposition in $Wo_{25}En_{31}Fs_{44}$ clinopyroxene. *Geol. Soc. Am.* **11**, 488 (abstr.).

Papike J. J (1998) *Planetary Materials, Reviews in Mineralogy.* 36.

Putnis A. (1992) *Introduction to Mineral Sciences.* Cambridge University Press. Mineralogical Society of America.

Robinson P., Ross M., Nord G. L., Smyth J. A., and Jaffe H. W. (1977) Exsolution lamellae in augite and pigeonite: Fossil indicators of lattice parameters at high temperature and pressure. *Am. Mineral.* **62**, 857–873.

Skrotzki W., Müller W. F., and Weber K. (1991) Exsolution phenomena in pyroxenes from the Balmuccia massif, NW-Italy. *Eur. J. Mineral.* **3**, 39–61.

Takeda H., Miyamoto M., Ishii T., and Lofgren G. E. (1975) Relative cooling rates of mare basalts at the Apollo 12 and 15 sites as estimated from pyroxene exsolution data. *Proc. 6th Lunar Planet. Sci. Conf.* 987–996.

Tullis J. and Yund R. A. (1979) Calculation of coherent solvi for alkali feldspar, iron-free clinopyroxene, nepheline-kalsilite, and hematite-ilmenite. *Am. Mineral.* **64**, 1063–1074.

Wagner C. (1961) Theorie der Alterung von Niederschlägen durch Umlösen (Ostwald-Reifung). *Zeitschrift für Elektrochemie.* **65**, 581–591.

Wagner R. and Kampmann R. (1991) Homogeneous second phase precipitation. In *Phase Transformations in Materials* (ed. P. Haasen), pp. 213–303. Verlag Chemie.

Watanabe S., Kitamura M., and Morimoto N. (1985) A transmission electron microscope study of pyroxene chondrules in equilibrated L-group chondrites. *Earth Planet. Sci. Lett.* **72**, 87–98.

Weinbruch S. and Müller W. F. (1995) Constraints on the cooling rates of chondrules from the microstructure of clinopyroxene and plagioclase. *Geochim. Cosmochim. Acta* **59**, 3221–3230.

Weinbruch S., Büttner H., and Rosenhauer M. (1992) The orthorhombic-hexagonal phase transformation in the system $BaCO_3$-$SrCO_3$ to pressures of 7000bar. *Phys. Chem. Minerals* **19**, 289–297.

Weinbruch S., Müller W. F., and Hewins R. H. (2001) A transmission electron microscope study of exsolution and coarsening in iron-bearing clinopyroxene from synthetic analogues of chondrules. *Meteoritics Planet. Sci.* **36**, 1237–1248.

Willaime C. and Brown W. L. (1974) A coherent elastic model for the determination of the orientation of exsolution boundaries: Application to the feldspars. *Acta Cryst.* **30**, 316–331.

Yund R. A. (1983) Alkali feldspar exsolution: Kinetics and dependence on alkali interdiffusion. In *Feldspars and Feldspathoids* (ed. W. L. Brown), pp. 281–315. Reidel.

Yund R. A. and Davidson P. (1978) Kinetics of lamellar coarsening in cryptoperthites. *Am. Mineral.* **63**, 470–477.